DOI: 10.1002/ejic.200800327

A T-Shaped μ_3-Oxido Trinuclear Iron Cluster with High Easy-Plane Anisotropy: Structural and Magnetic Characterization

Pablo Alborés*[a] and Eva Rentschler*[a]

Keywords: Polynuclear complexes / Magnetic properties / DFT calculations / (μ-Oxido)iron core / Easy-plane anisotropy

The synthesis, crystal structure and magnetochemical characterization of a new μ-oxido trinuclear iron cluster (old nomenclature: μ-oxo trinuclear iron cluster), $[Fe_3(\mu_3\text{-}O)(\mu_2\text{-}CH_3O)_2(\mu_2\text{-}CH_3COO)_2(phen)_2Cl_3]$, is reported. The reaction of hydrated $FeCl_3$ with sodium acetate and 1,10-phenanthroline in a mixture of methanol and acetonitrile afforded crystals suitable for X-ray crystallographic determination. The new compound crystallizes in the tetragonal $I4_1/a$ space group ($a = b = 13.6322$ Å, $c = 37.3538$ Å, $Z = 8$, $V = 6941.7$ Å^3). The core of the complex is an isosceles triangle bridged by a μ_3-O ion with a rare T-shaped geometry. The chloride ions are bound terminally, and the phenanthroline ligands are π-stacked. Variable-temperature solid-state dc magnetization studies were carried out in the 2.0–300 K range. Data were fit with an isotropic Heisenberg spin Hamiltonian, which included an axial anisotropy (zero-field splitting) term. Two antiferromagnetic exchange parameters for the isosceles triangle arrangement of the iron ion were needed, with values of –11.2 and –47.7 cm^{-1}, while a positive D value of about 1.5 cm^{-1} was obtained. In addition, magnetization (M) vs. field (H) and temperature (T) data established an $S_T = 5/2$ ground-state spin. We also performed broken-symmetry DFT calculations, which reproduced the experimental J values and the ground-state spin well. The replacement of one Fe^{3+} ion by a Ga^{3+} ion allowed for simplification of the three-centre problem to one treating a dinuclear exchange-coupled system, and this afforded good computed values. To the best of our knowledge, this is the first time that this specific replacement has been applied within broken-symmetry DFT calculations.

Introduction

Polynuclear iron compounds containing oxygen-based ligands are relevant to a variety of fields, a central one being magnetic materials. Nowadays, several groups develop synthetic methods that yield new polynuclear Fe–O clusters. The paramagnetic nature of Fe in its common oxidation states often leads to interesting magnetic properties for polynuclear Fe clusters, such as high ground-state spin values, which can possibly lead to single-molecule magnetism.[1] Almost all exchange interactions between Fe^{III} centres are antiferromagnetic. However, certain Fe_x topologies can possess large ground-state spin values as a result of spin frustration. Spin frustration is defined by competing exchange interactions of comparable magnitude, which prevent (frustrate) the preferred antiparallel alignment of all spins and hence afford larger ground-state spin values than might be predicted.[2] In some cases, where these large ground-state spins are coupled to a significant magnetic anisotropy, the compounds can behave as single-molecule magnets (SMMs). This is the case for SMMs such as $[Fe_8O_2(OH)_{12}(tacn)_6]^{8+}$, $[Fe_4(OMe)_6(dpm)_6]$, etc.[3]

A common synthetic approach is based on the auto-assembly of the most stable cluster under specific reaction conditions, which usually involve the mixing of simple iron salts with chelating ligands in polar solvents under aerobic conditions and without moisture exposure prevention. Using this approach for the reaction of hydrated $FeCl_3$ with sodium acetate and the bidentate 1,10′-phenanthroline ligand in an acetonitrile/methanol mixture, we obtained a new μ-oxido trinuclear Fe_3O core, $[Fe_3(\mu_3\text{-}O)(\mu_2\text{-}CH_3O)_2(\mu_2\text{-}CH_3COO)_2(phen)_2Cl_3]$, with an uncommon T-shaped arrangement. There have only been a few examples of this type of atomic arrangement in oligonuclear complexes reported up to now.[4–7] In the present work, we report the synthesis and structural characterization results as well as a combined experimental and computational study of the magnetic behaviour of this new iron cluster.

Results and Discussion

Synthesis and Structural Characterization

The reaction of ferric chloride in the presence of methanol, with the bidentate 1,10-phenanthroline ligand and a carboxylate source, in this case sodium acetate, afforded a

[a] Institute of Inorganic and Analytical Chemistry, Johannes Gutenberg University of Mainz,
Duesbergweg 10–14, 55128 Mainz, Germany
Fax: +49-6131-39-23922
E-mail: albores@uni-mainz.de
rentschl@uni-mainz.de

Supporting information for this article is available on the WWW under http://www.eurjic.org or from the author.

new T-shaped (μ-oxido)triiron cluster in a reasonable yield. In spite of its simplicity, this is only the fifth structurally characterized compound exhibiting this atomic arrangement. Undoubtedly, the extended planarity of the phenanthroline rings plays a key role in the architecture of this compound, as, in contrast, we were unable to isolate the analogous complex bearing 2,2′-bipyridine.

The complex crystallizes in the tetragonal space group $I4_1/a$ (Figure 1), and individual molecules appear well isolated, as can be noticed in the crystal packing (Fe···Fe intermolecular distance > 8 Å) (Figure 1b). The most remarkable features are the π stacking of the phenanthroline ligands, which forces the arrangement of the $\{Fe_3O\}$ core into a nearly perfect isosceles triangle and the arrangement of all the terminal chlorido ligands into a *trans* configuration with respect to the central μ-oxido ligand (Figure 1a). The presence of a crystallographically imposed twofold rotation axis causes the Fe atoms bound to the phenanthroline ligands as well as their coordination spheres to be completely equivalent. This is a unique characteristic among T-shaped Fe_3O-related compounds that have already been structurally characterized.[4–7] The coexistence of long and short Fe–μ-O bond lengths is crucial for the T-shaped arrangement. The shorter Fe1–O1 bond of 1.902 Å is one of the largest within the small group of T-shaped Fe_3O cores, which have Fe–O distances ranging between 1.865 and 1.919 Å. In contrast, the longer Fe2–O1 distance of 1.985 Å is one of the shortest among analogous bond lengths in this group, which range from 1.934 to 2.070 Å. In addition, the present complex is the one out of the group that most closely bears an ideal T-shaped geometry. Its Fe2–O–Fe2′ angle of 163.89° is slightly larger than 162.83°, which was observed in the recently reported Fe_3O T-shaped compound containing azide ions.[7] The smallest angle observed within the group is 152.07 Å.[6]

In contrast to the other related Fe_3O compounds, all additional bridging ligands in the reported complex bear an O donor atom, as is the case for the acetate and methoxide ions. The Fe–O distances are not equivalent for either the acetate or the methoxide ion, which shows a remarkable asymmetry (see Table 1). The shorter distance is observed for both ligands where the Fe atom involved is coordinated to the phenanthroline ring. This result probably reflects the higher electron-accepting nature of phenanthroline in comparison with the other ligands present in the complex. The $Fe–O_{acetate}$ distances are comparable to the typical values observed in the $[Fe_3O(AcO)_6L_3]$ compounds,[8] while the $Fe–O_{methoxide}$ distance is also within the typical range observed in other clusters containing the $Fe_3(\mu_2\text{-}CH_3O)(\mu_3\text{-}O)$ motif.[9,10]

Noticeably, the T-shaped pattern extends up to the terminal Cl ions, $\{Cl_3Fe_3(\mu_3\text{-}O)\}$. This moiety is the first example reported so far for trinuclear species, and it is still scarcely found among polynuclear Fe clusters. The few examples reported comprise mainly cubane-type structures, where the Fe–O bond is excessively long (>2.2 Å) and the Fe–Cl bond length ranges between 2.20 and 2.26 Å.[10] In our reported complex, the Fe–O bond length is quite short and the observed Fe–Cl bond lengths therefore appear quite large (>2.3 Å), which reflects an important electronic repulsion along the Fe–O–Cl axis. In fact, the shorter Fe–O distance correlates with the longer Fe–Cl one (see Table 1).

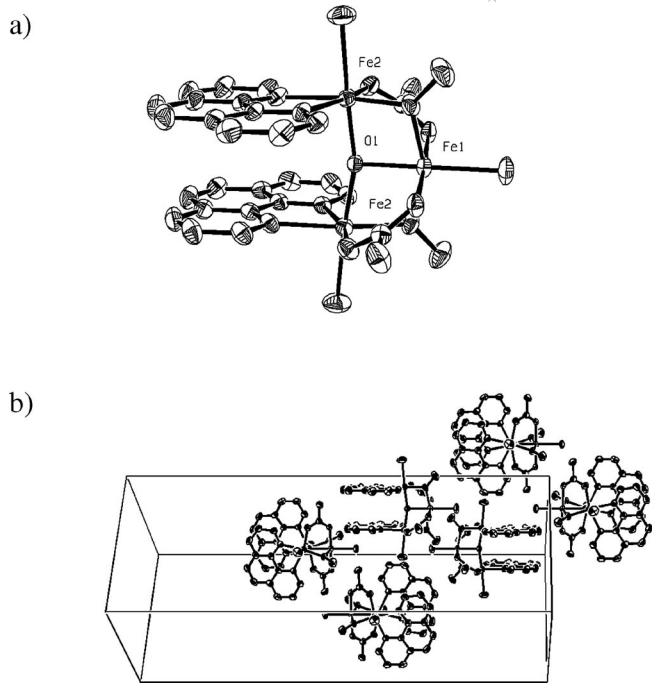

Figure 1. (a) Top: ORTEP (50% probability) plot of the trinuclear μ_3-oxido complex in the crystal structure showing the T-shaped core. (b) Bottom: view of the molecules packing in the tetragonal cell.

Table 1. Selected bond angles and distances of the reported complex.

Distance [Å]		Angle [°]	
Fe1–O1	1.985(3)	Fe2–O1–Fe2′	163.89(15)
Fe2–O1	1.9022(5)	Fe1–O1–Fe2	98.06(8)
Fe1–Cl1	2.2994(12)	Cl1–Fe1–O1	180.00(0)
Fe2–Cl2	2.3561(9)	Cl2–Fe2–O1	175.35(6)
Fe2–O2	1.9747(19)		
Fe1–O2	1.9883(19)		
Fe1–O3	2.1022(19)		
Fe2–O4	2.013(2)		
Fe2–N1	2.166(2)		
Fe2–N2	2.168(2)		

The Fe–N bond lengths are comparable to the distances observed in other (μ-oxido)Fe complexes bearing phenanthroline. The presence of the π stacking between the two phenanthroline rings is a common feature for this ligand. The stacking distance of about 3.6 Å, similar to that observed in other Fe complexes,[11] agrees well with the Fe2–Fe2′ distance of 3.767 Å.

Magnetic Properties

The magnetic behaviour of the reported complex was studied over the 2–300 K temperature range (Figure 2) under an applied field of 1 T. The $\chi_m T$ value at 300 K of

5.24 $cm^3 K mol^{-1}$ is well below the expected value for three isolated high-spin Fe^{III} ions, 13.12 $cm^3 K mol^{-1}$, which indicates strong antiferromagnetic interactions within the complex. With decreasing temperature, χT steadily decreases to reach a minimum of 3.66 $cm^3 K mol^{-1}$ at 48 K, after which it increases to a maximum of 3.76 $cm^3 K mol^{-1}$ at 4 K to finally plummet below 4 K.

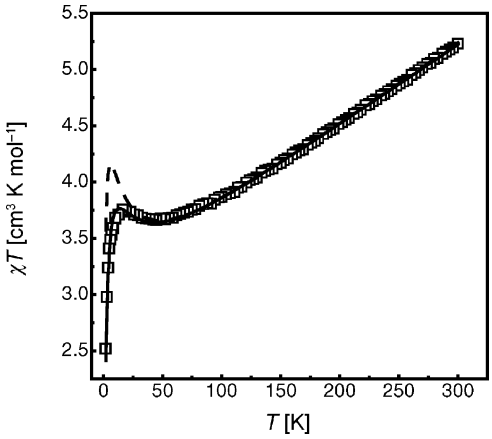

Figure 2. χT vs. T plot at 1 T of a powdered sample of $[Fe_3(\mu_3\text{-}O)(\mu_2\text{-}CH_3O)_2(\mu_2\text{-}CH_3COO)_2(phen)_2Cl_3]$. Dashed line: best fit with Hamiltonian of Equation (2) (see text), J_a = –11.5 cm^{-1}, J_b = –46.4 cm^{-1}, g_{fixed} = 2.0; solid line: best fit with Hamiltonian of Equation (2) with an added zfs term as in Equation (4) (see text), J_a = –11.2 cm^{-1}, J_b = –47.7 cm^{-1} and D = 1.43 cm^{-1}.

This behaviour is typical for spin-frustrated systems with competing antiferromagnetic exchange interactions. Hence we attempted a full fitting of the data by obtaining the energy of the different spin states and calculating the molar susceptibility with Equation (1) for all possible field orientations:

$$\chi = \frac{1}{H}\frac{N\sum_n(-\partial E_i/\partial H)\exp(-E_i/kT)}{\sum_i \exp(-E_i/kT)} \quad (1)$$

The energy of the different spin levels is obtained through diagonalization of the suitable Hamiltonian. In this case, the Heisenberg spin Hamiltonian describing the isotropic exchange interactions within an isosceles Fe3 triangle of C_2 symmetry (Figure 3) is given by Equation (2), where J_a refers to the interactions between Fe1···Fe2 and Fe1···Fe2′, J_b refers to the Fe2···Fe2′ interaction and S_i refers to the spin of atom i:

$$H = -2J_a(\hat{S}_1\hat{S}_2 + \hat{S}_1\hat{S}_3) - 2J_b(\hat{S}_2\hat{S}_3) \quad (2)$$

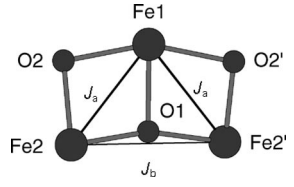

Figure 3. T-Shaped Fe_3O core of the reported complex showing the pairwise exchange interactions.

The energies of the resultant total spin states, S_T, which are eigenfunctions of the Hamiltonian in this coupling scheme, are given by Equation (3), where $S_A = \hat{S}_2 + \hat{S}_3$. The overall multiplicity of the spin system is 216, and this is made up of 27 individual spin states ranging from S_T = 1/2 to S_T = 15/2.

$$E|S_T,S_A\rangle = -J_a[S_T(S_T + 1) - S_A(S_A + 1)] - J_b[S_A(S_A + 1)] \quad (3)$$

The best fit of the χT vs. T plot with the Hamiltonian in Equation (2) with an added Zeeman term, J_a and J_b as fit parameters, and an isotropic g value fixed to 2.0, afforded values of J_a = –11.5 cm^{-1} and J_b = –46.4 cm^{-1}. This fit is shown as a dashed line in Figure 2. It is possible to obtain a good fit only down to 16 K; below this temperature the calculated χT values deviate noticeably from the experimental data. The J values obtained from Equation (3) afforded a ground state of S_T = 5/2, which in the coupling scheme corresponds to the ket $|S_T,S_A\rangle = |5/2,0\rangle$. The antiferromagnetic interaction J_a competes unfavourably with the much stronger J_b interaction. The big difference between the two exchange coupling constants can be rationalized in terms of the different Fe–O bond lengths, as was done for the recently reported related T-shaped complex, $[Fe_3O(O_2CtBu)_2(N_3)_3(dmem)_2]$.[7] In fact, these values of J_a and J_b are in agreement with those found for the latter compound as well as the other magnetically characterized T-shaped Fe_3O complex, $[Fe_3O(TIEO)_2(O_2CPh)_2Cl_3]$,[4] which are –3.6 cm^{-1} and –8 cm^{-1} for J_a and –45.9 cm^{-1} and –55 cm^{-1} for J_b, respectively.

In spite of this convincing magnetic interpretation, we attempted to understand the origin of the deviation at low temperature in the fit of the χT vs. T plot. We found that an excellent and reliable fit of the experimental data is obtained if an axial zero-field splitting (zfs) term is added to the Hamiltonian of Equation (2) that takes into consideration the local zfs contribution, D_i, of the Fe^{III} ions, as shown in Equation (4).

$$H_{zfs} = \sum_i D_i[\hat{S}^2_{z,i} - S_i(S_i + 1)/3] \quad (4)$$

The resulting fit over the whole 2–300 K temperature range, with the improved Hamiltonian, J_a, J_b and D_i fit parameters and the isotropic g value fixed at 2.0, is shown in Figure 2 as the solid line. It gave an agreement factor, $R = 1/(N - n_p)[\Sigma(\chi_{calc}T - \chi_{obs}T)^2/\Sigma(\chi_{obs}T)^2]^{1/2}$, of 7.8×10^{-5}, where N is the number of experimental points and n_p is the number of parameters. The new parameters obtained are J_a = –11.2±0.1 cm^{-1}, J_b = –47.7±0.4 cm^{-1} and D = 1.43±0.06 cm^{-1} (errors at 95% confidence level). The J values are almost identical to those obtained without the inclusion of the zfs term, which reinforces our S_T ground state assignment. The key point now is the reliability of the D value obtained, as it is well known that it is usually not possible to get an accurate estimation of either this parameter or its sign from susceptibility measurements alone. This does not seem to be the case here, as a very deep minimum

is observed in the g vs. D error contour plot for the fit, as is shown in Figure 4, which completely discards the possibility of a negative value for the zfs parameter. The J_a vs. J_b error surface is also reported as additional evidence (Figure S1). It is important to remark at this point that there is no possibility of obtaining the D value from the Fe2 and Fe2′ ions, as they are not contributing to the resulting ground state $|5/2,0\rangle$. In fact, the fitting improvement is only dependent on the Fe1 D value.

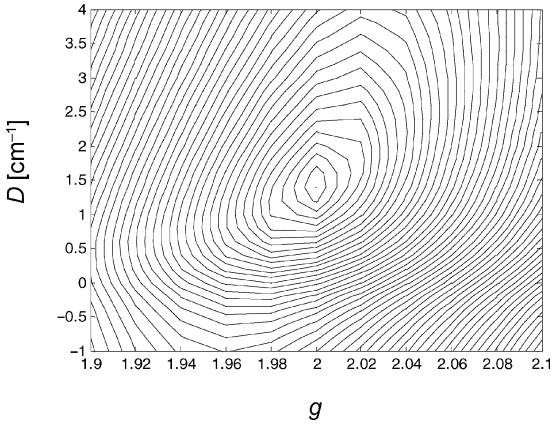

Figure 4. D vs. g error contour for the simulation of the χT vs. T plot with J_a = –11.2 cm^{-1} and J_b = –47.7 cm^{-1} fixed.

In order to reinforce our assessment of the zfs and the S_T ground state values in this T-shaped Fe_3O complex, we performed variable-field (H) and variable-temperature magnetization (M) measurements. Data were collected over the 0.5–4.0 T and 2–50 K ranges. The resulting data are plotted in Figure 5 as reduced magnetization ($M/N\beta$) vs. H/T, where N is Avogadro's number and β is the Bohr magneton. The saturation value at the highest field and lowest temperatures is 4.0 $N\beta$, which is below the expected gS value of 5 (g = 2.0) arising from the Brillouin function. This observation, together with the nonsuperimposable isofield curves, reveals the existence of a non-negligible zfs contribution. The data were fit by diagonalization of the spin Hamiltonian matrix, under the assumption that only the ground state is populated, by incorporating axial anisotropy and Zeeman terms, and by employing a full powder average. The corresponding spin Hamiltonian is given by Equation (5).

$$H = D[\hat{S}_z^2 - S(S + 1)/3] + g\beta\hat{S}H \quad (5)$$

The best fit is obtained for S = 5/2, with the isotropic g fixed at 2.0 and D = 1.47±0.08 cm^{-1} (solid line in Figure 5), $R = 3.9 \times 10^{-4}$. If the g value is not fixed, the optimum fit parameter falls below 1.9 and is hence not physically reasonable for a high-spin Fe^{III} ion. There is no possibility of obtaining the observed saturation value of 4.0 $N\beta$ with negative values of D. The obtained D value is in very good agreement with that obtained from the fitting of the χT vs. T plot. Additionally, we performed a magnetization vs. field measurement at 4 K to observe mainly the S_T = 5/2 ground-state behaviour (first excited state $|S_T,S_A\rangle$ = $|3/2,1\rangle$ at 20 cm^{-1}) (Figure S2). The theoretical curve (shown as a solid line) with the same Hamiltonian from Equation (5) and

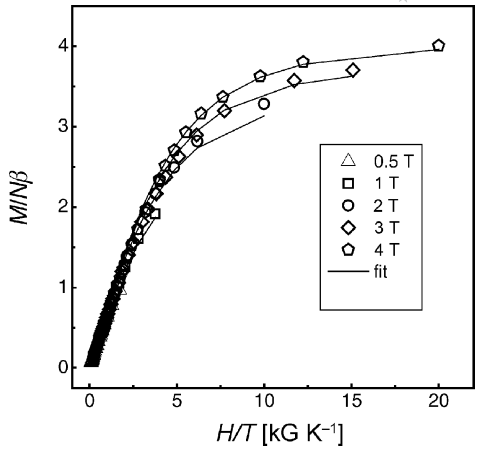

Figure 5. Plot of reduced magnetization ($M/N\beta$) vs. H/T for the reported complex. The solid lines represent the fitting of the data with parameters: S = 5/2 (fixed), g = 2.0 (fixed) and D = 1.4 cm^{-1} (see text).

with S = 5/2, an isotropic fixed g value of 2.0 and D = 1.4 cm^{-1} is in good agreement with the experimental plot data.

All our results strongly support an S_T = 5/2 ground state with an easy-plane positive D parameter above 1 cm^{-1} for this new T-shaped Fe_3O core. This zfs value contradicts that found for the closely related compound, $[Fe_3O(O_2C\,t\mathrm{Bu})_2(N_3)_3(\mathrm{dmem})_2]$, which exhibits a negative D value of about –0.8 cm^{-1}.[7] However, this latter value is obtained from a fitting procedure which uses an unrealistic g value of 1.9 for a high-spin Fe^{III} high system.

The non-easy axis type D value observed for our complex precludes its potential behaviour as a single-molecule magnet but not as a source of anisotropy for building up higher nuclearity systems.

DFT Calculations

Analysis of the orbitals involved in the coupling between the Fe^{III} ions predicts an antiferromagnetic coupling, as observed. The exchange coupling constants, J_a and J_b, obtained from a broken-symmetry (BS) analysis on the crystallographic geometry using the two different approaches described in the experimental section are presented in Table 2. They agree surprisingly well with the experimental ones: the J_b value is almost identical to that obtained from the fitting, while the J_a value is somewhat underestimated, most remarkably with method 2 (see Experimental Section).

Table 2. Summary of broken-symmetry DFT calculations.

	Calculated J values J_a/J_b [cm^{-1}]	HS-state Mulliken spin densities Fe1/Fe2/Fe2′
Method 1	–10.9/–52.9 (Yamaguchi[a]) –9.1/–44.2 (non-projected[a]) –10.9/–53.1 (projected[a])	4.070/4.053/4.053
Method 2	–3.8/–53.4 (non-projected[a]) –4.6/–54.8 (projected[a])	–0.002/4.062/4.062[b] 4.067/4.042/0.006

[a] See Experimental Section. [b] The value close to zero corresponds to a Ga^{III} ion.

This can be understood by taking into consideration that this method involves the solving of linear equations with dependent J values, which leads to more uncertainty possibilities due to propagated errors. In both cases, the right ground state of $S_T = 5/2$ is predicted, as can be checked by the utilization of Equation (3).

The observation of nearly identical Mulliken spin densities at the Fe sites for the high-spin (HS) state with both methods (Table 2) supports the robustness of method 1, which relies on the replacement of an Fe^{III} ion with a Ga^{III} ion as a means of reducing the number of exchange interactions present in the cluster. The correct description of the different broken-symmetry states in the case of method 2 is confirmed by inspection of the total spin density obtained (see Figure S4 for spin density plots of method 1). Figure 6 shows the different spin topologies that arise from the spin-flipping of the different Fe^{III} sites.

The calculated corresponding orbitals (COs) with overlap values smaller than one are displayed in Figure 7. As discussed in the literature, these pairs of orbitals correspond

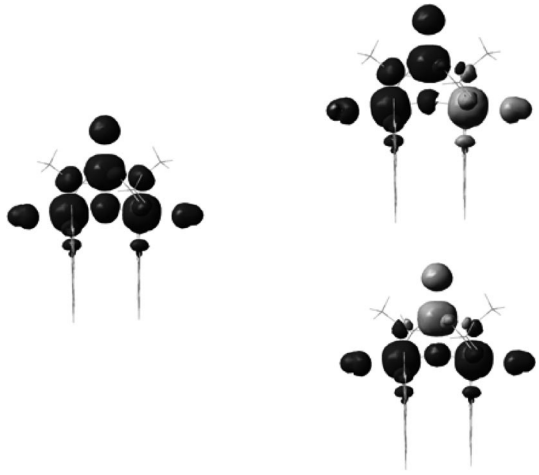

Figure 6. Spin density surfaces (isogrid = 0.004 a.u.) of the high-spin state (left) and the broken-symmetry states (right) from DFT calculations with method 2. Dark areas correspond to positive spin density values, and light areas to negative spin density values.

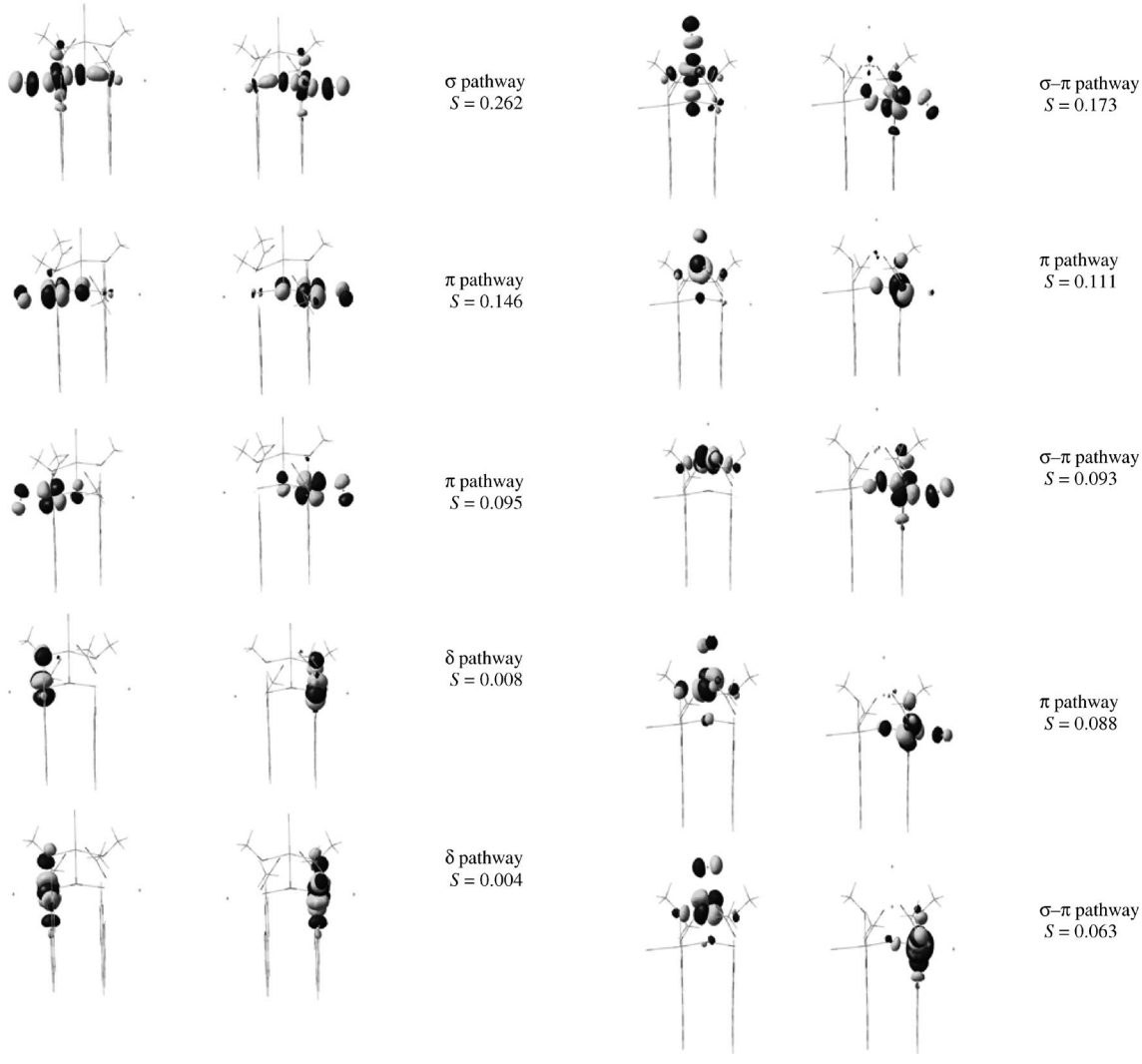

Figure 7. Corresponding orbitals arising from broken-symmetry DFT calculations with method 2 showing the exchange coupling pathways between magnetic orbitals and their overlaps.

to the non-orthogonal magnetic orbitals of the broken-symmetry UHF solution, whereas those cases with overlap values close to one identify normal UHF solutions with some spin polarization.[12]

For calculations performed with method 1, two decoupled exchange pathways can be analyzed: one involving the symmetry related Fe2···Fe2′ interaction and one involving the Fe1···Fe2 interaction. Inspection of the COs for the former interaction reveals three main antiferromagnetic pathways (S = 0.262, 0.146 and 0.095), where one is of a σ nature and the other two are of a π nature. In all of them, exchange coupling exists mainly through the oxido bridging ligand. The remaining two pairs of COs contribute only marginally to the coupling, as they are of δ nature. For the Fe1···Fe2 interaction, the five existing pathways contribute rather evenly, but with a lower overall overlap between magnetic orbitals relative to the Fe2···Fe2′ case. This can be well understood as there are no pure σ pathways, only π or mixed σ–π ones, due to the almost 90° angle between the two Fe sites.

The orbital analysis that arises from calculations carried out by method 2 (Figure S3) is not as straightforward. In this case, the two exchange interactions are not decoupled, and this is reflected in the composition of the COs. The COs arising from the broken-symmetry state where the spin density was flipped in Fe1 illustrates the frustrated antiferromagnetic interactions pretty well. The strongly coupled Fe2···Fe2′ interaction (through J_b) constitutes one set of five magnetic orbitals that also interact antiferromagnetically (J_a) with the magnetic orbitals located on Fe1. COs arising from the other possible broken-symmetry state in which the spin density is flipped on one of the symmetry-related Fe2(Fe2′) atoms, are much more mixed, and both sets of magnetic orbitals contain contributions from J_a and J_b. To the best of our knowledge, this is the first example where a corresponding orbital transformation is applied to understand the exchange pathways in a frustrated Fe_3O spin system and where an Fe^{III} ion is replaced with a diamagnetic Ga^{III} ion as a means of simplifying the exchange coupling pattern.

Conclusions

We have succeeded in the preparation of a new example of the very rare T-shaped Fe_3O clusters. We have established its S_T = 5/2 ground-state spin, arising from two rather strong, unevenly competing antiferromagnetic interactions between the Fe centres. In addition, we have shown that this ground state exhibits high easy-plane anisotropy with $D > 1\ cm^{-1}$. A reliable value for this parameter was obtained from powder susceptibility and magnetization measurements analysis, which is unusual for this type of determination. The projected D value corresponds exclusively (neglecting dipolar and anisotropic exchange contributions) with the local value of the Fe1 site, as determined from the spin-coupling pattern arising from the J_a/J_b ratio. The DFT calculations reproduce these results well. The magnetic orbital representation by means of the corresponding orbital transformation nicely illustrates the considerably different antiferromagnetic interactions. Additionally, we have successfully applied a calculation tool within the broken-symmetry framework, which consists of the replacement of an Fe atom by a Ga atom to reduce the three-centre problem to an equivalent problem which treats a more simple dinuclear exchange-coupled system. In spite of it being well known that a negative D value is necessary for developing single-molecule magnet behaviour, a suitable combination of clusters with high, positive D values can be used to build up new high-spin clusters with total easy-axis anisotropy. The new reported Fe_3O moiety can be envisioned as a new building block for this purpose.

Experimental Section

Materials and Physical Measurements: All chemicals were reagent grade and used as received without further purification. C, H and N analysis was performed on a Foss Heraeus Vario EL elemental analyzer. Infrared spectra were recorded with a Jasco FT-IR 4200 spectrophotometer with KBr pellets in the 400–4000 cm^{-1} range.

Preparation of $[Fe_3(\mu_3\text{-}O)(\mu_2\text{-}CH_3O)_2(\mu_2\text{-}CH_3COO)_2(phen)_2Cl_3]$: $FeCl_3{\cdot}6H_2O$ (0.42 g, 1.5 mmol) and $NaCH_3COO{\cdot}4H_2O$ (0.32 g, 2.3 mmol) were dissolved in a methanol/acetonitrile mixture (10:30 mL). 1,10-phenanthroline monohydrate (0.16 g, 0.8 mmol) dissolved in acetonitrile (30 mL) was added. The resulting deep red solution was stirred for about ten minutes and then filtered. The filtrate was left standing at room temp. After 2–3 d, block-shaped red crystals of the product were obtained. One of them was used for X-ray crystallographic determination, and the rest of them were collected by filtration, washed with acetonitrile and vacuum dried. Yield: 0.16 g, 38% (Fe based). $C_{30}H_{28}Cl_3Fe_3N_4O_7$ (830.46): calcd. C 43.39, H 3.40, N 6.75; found C 43.75, H 3.49, N 7.41.

Magnetic Measurements: Magnetic measurements were performed with a Quantum Design MPMS-7 SQUID magnetometer. All experimental magnetic data were corrected for the diamagnetism of the sample holders and of the constituent atoms (Pascal's tables).

X-ray Crystallographic Structure Determination: The crystal structure was determined with a Bruker Smart APEX II CCD area-detector diffractometer using graphite-monochromated Mo-K_α radiation (λ = 0.71073 Å) at 100 K. Data were corrected for absorption with PLATON[13] using a multiscan semi-empirical method. The structure was solved by direct methods with SHELXS-97[14] and refined by full-matrix least-squares on F^2 with SHELXL-97.[15] Hydrogen atoms were added geometrically and refined as riding atoms with a uniform value of U_{iso}. Final crystallographic data and values of R_1 and wR are listed in Table 3, while the main angles and distances are listed in Table 1. CCDC-683068 contains the supplementary crystallographic data for this paper. These data can be obtained free of charge from the Cambridge Crystallographic Data Centre via www.ccdc.cam.ac.uk/data_request/cif.

Quantum Chemical Calculations: Density functional theory (DFT) spin-unrestricted calculations were performed using the Gaussian03 program (revision D.01)[16] at the B3LYP level employing the LanL2DZ basis set. Tightly converged (10^{-8} Eh in energy) single-point calculations at the X-ray geometry were performed in order to analyze the exchange coupling between the iron centres. The methodology applied here relies on the broken-symmetry formalism, originally developed by Noodleman for SCF

Table 3. Crystal data and structure refinement results for $[Fe_3(\mu_3\text{-}O)(\mu_2\text{-}CH_3O)_2(\mu_2\text{-}CH_3COO)_2(phen)_2Cl_3]\ H_2O$.

Empirical formula	$C_{30}H_{28}Cl_3Fe_3N_4O_8$
Formula weight [g mol^{-1}]	846.46
Temperature [K]	173(2)
Crystal system	tetragonal
Space group	$I4_1/a$ (No. 88)
Unit cell dimensions[a]	
$a = b$ [Å]	13.6322(2)
c [Å]	37.3538(7)
Volume [Å^3]	6941.7(3)
Z, calculated density [Mg m^{-3}]	8, 1.620
Absorption coefficient [mm^{-1}]	1.522
F(000)	3432
Crystal size [mm]	$0.25 \times 0.25 \times 0.09$
Crystal colour/shape	red/block
Radiation, graphite monochromator	Mo-K_α, λ = 0.71073 Å
θ range data collection [°]	1.59 to 27.85
Index ranges	$-17 \le h \le 12$, $-16 \le k \le 17$, $-45 \le l \le 49$
Reflections collected/unique	38349/4133 [R(int) = 0.0631]
Observed reflections [$I > 2\sigma(I)$]	2714
Completeness [%]	99.9 (to θ = 27.85°)
Max. and min. transmission	0.8912 and 0.6763
Refinement method	full-matrix least squares on F^2
Weights, w	$[\sigma^2(F_o^2) + (0.034P)^2 + 10.15P]^{-1}$ $P = [\mathrm{Max}(F_o^2,0) + 2F_c^2]/3$
Data/restraints/parameters	4133/0/214
Goodness-of-fit on F^2	0.975
Final R-index [$I > 2(I)$][b]	R_1 = 0.0421, wR_2 = 0.1148
R indices (all data)	R_1 = 0.071, wR_2 = 0.1232
Largest peak and hole [e Å^{-3}]	0.876 and –0.471

[a] Least-squares refinement of the angular settings for 10694 reflections in the $3.04° < \theta < 26.00°$ range. [b] R indices defined as: $R_1 = \Sigma||F_o| - |F_c||/\Sigma|F_o|$, $wR_2 = [\Sigma w(F_o^2 - F_c^2)^2/\Sigma w(F_o^2)^2]^{1/2}$.

methods,[17] which involves a variational treatment within the restrictions of a single spin-unrestricted Slater determinant built upon using different orbitals for different spins. This approach has been later applied within the framework of DFT. The HS and BS energies were then combined in order to estimate the exchange coupling parameter J involved in the widely used Heisenberg–Dirac–van Vleck Hamiltonian:

$$\hat{H}_{HDvV} = -2J\hat{S}_A\hat{S}_B$$

We carried out two different approaches within the broken-symmetry framework. (1) We first replaced one of the Fe atoms with the diamagnetically equivalent main group Ga atom as a means to obtain a model dinuclear system wherein the two different exchange interactions could be isolated and evaluated. We employ here the approximation described by Yamaguchi and co-workers,[18] who relate the exchange coupling parameter to the energies and expectation values of the spin-squared operator for the HS ($M_S = S_A + S_B$) and BS ($M_S = |S_A - S_B|$) states.

$$J = -\frac{E_{HS} - E_{BS}}{<\hat{S}^2_{HS}> - <\hat{S}^2_{BS}>}$$

In the second approach (2), we calculated the two possible spin topologies of broken-symmetry nature, from which the two different exchange coupling values could be obtained after considering the individual pair-like spin interactions involved in the description of the different broken-symmetry states. The energy difference between the HS and BS states for this methodology can be obtained from the non-projected formula:[19]

$E_{BS} - E_{HS} = 2J_{12}(2S_1S_2 + S_2)$, with $S_2 > S_1$

or from the projected one:[20]

$E_{BS} - E_{HS} = 2J_{12}(2S_1S_2)$

We also employed the BS-type spin-unrestricted solutions after a corresponding orbital transformation as a means to visualize the interacting non-orthogonal magnetic orbitals.[12,21] We remark that these orbitals do not have a well-defined orbital energy. For this reason, the figures showing such orbitals do not give orbital energies explicitly, but just their overlapping magnitudes as well as the spin coupling exchange pathways.

We notice that a most rigorous theoretical treatment in the calculation of the exchange coupling constants within broken-symmetry formalism could be performed by means of separate geometry optimizations of the HS and BS states.[22] However, this is beyond the aim of this work.

Supporting Information (see footnote on the first page of this article): J_a vs. J_b error contour plot (Figure S1), reduced magnetization vs. field at 4 K (Figure S2), corresponding orbitals arising from DFT calculations with method 1 (Figure S3), total spin density plots from the different spin states arising from DFT calculations with method 1 (Figure S4).

Acknowledgments

We gratefully acknowledge the Alexander von Humboldt Foundation for granting a research fellowship.

[1] a) G. Christou, D. Gatteschi, D. N. Hendrickson, R. Sessoli, *MRS Bull.* **2000**, *25*, 66–71; b) D. Gatteschi, A. Caneschi, R. Sessoli, A. Cornia, *Chem. Soc. Rev.* **1996**, *25*, 101–109.

[2] a) J. K. McCusker, J. B. Vincent, E. A. Schmitt, M. L. Mino, K. Shin, D. K. Coggin, P. M. Hagen, J. C. Huffman, G. Christou, D. N. Hendrickson, *J. Am. Chem. Soc.* **1991**, *113*, 3012–3021; b) A. K. Powell, S. L. Heath, D. Gatteschi, L. Pardi, R. Sessoli, G. Spina, F. Delgiallo, F. Pieralli, *J. Am.*

Chem. Soc. **1995**, *117*, 2491–2502; c) O. Kahn, *Chem. Phys. Lett.* **1997**, *265*, 109–114; d) L. F. Jones, E. K. Brechin, D. Collison, M. Helliwell, T. Mallah, S. Piligkos, G. Rajaraman, W. Wernsdorfer, *Inorg. Chem.* **2003**, *42*, 6601–6603; e) C. Canada-Vilalta, T. A. O'Brien, E. K. Brechin, M. Pink, E. R. Davidson, G. Christou, *Inorg. Chem.* **2004**, *43*, 5505–5521; f) A. M. Ako, O. Waldmann, V. Mereacre, F. Klower, I. J. Hewitt, C. E. Anson, H. U. Gudel, A. K. Powell, *Inorg. Chem.* **2007**, *46*, 756–766; g) J. Overgaard, E. Rentschler, G. A. Timco, N. V. Gerbeleu, V. Arion, A. Bousseksou, J. P. Tuchagues, F. K. Larsen, *J. Chem. Soc., Dalton Trans.* **2002**, 2981–2986; h) J. Overgaard, D. E. Hibbs, E. Rentschler, G. A. Timco, F. K. Larsen, *Inorg. Chem.* **2003**, *42*, 7593–7601.

[3] a) C. Delfs, D. Gatteschi, L. Pardi, R. Sessoli, K. Wieghardt, D. Hanke, *Inorg. Chem.* **1993**, *32*, 3099–3103; b) C. Sangregorio, T. Ohm, C. Paulsen, R. Sessoli, D. Gatteschi, *Phys. Rev. Lett.* **1997**, *78*, 4645–4648; c) A. L. Barra, A. Caneschi, A. Cornia, F. F. de Biani, D. Gatteschi, C. Sangregorio, R. Sessoli, L. Sorace, *J. Am. Chem. Soc.* **1999**, *121*, 5302–5310; d) D. Gatteschi, R. Sessoli, A. Cornia, *Chem. Commun.* **2000**, 725–732; e) G. W. Powell, H. N. Lancashire, E. K. Brechin, D. Collison, S. L. Heath, T. Mallah, W. Wernsdorfer, *Angew. Chem. Int. Ed.* **2004**, *43*, 5772–5775; f) Y. Pontillon, A. Caneschi, D. Gatteschi, R. Sessoli, E. Ressouche, J. Schweizer, E. Lelievre-Berna, *J. Am. Chem. Soc.* **1999**, *121*, 5342–5343.

[4] S. M. Gorun, G. C. Papaefthymiou, R. B. Frankel, S. J. Lippard, *J. Am. Chem. Soc.* **1987**, *109*, 4244–4255.

[5] M. Hirotsu, M. Kojima, W. Mori, Y. Yoshikawa, *Chem. Lett.* **1999**, 229–230.

[6] T. Kajiwara, T. Ito, *Angew. Chem. Int. Ed.* **2000**, *39*, 230–233.

[7] R. Bagai, S. Datta, A. Betancur-Rodriguez, K. A. Abboud, S. Hill, G. Christou, *Inorg. Chem.* **2007**, *46*, 4535–4547.

[8] a) C. E. Anson, J. P. Bourke, R. D. Cannon, U. A. Jayasooriya, M. Molinier, A. K. Powell, *Inorg. Chem.* **1997**, *36*, 1265–1267; b) W. Hibbs, P. J. van Koningsbruggen, A. M. Arif, W. W. Shum, J. S. Miller, *Inorg. Chem.* **2003**, *42*, 5645–5653; c) S. Supriya, S. Mankumari, P. Raghavaiah, S. K. Das, *New J. Chem.* **2003**, *27*, 218–220.

[9] a) A. Caneschi, A. Cornia, A. C. Fabretti, D. Gatteschi, W. Malavasi, *Inorg. Chem.* **1995**, *34*, 4660–4668; b) A. Caneschi, A. Cornia, A. C. Fabretti, D. Gatteschi, *Angew. Chem. Int. Ed. Engl.* **1995**, *34*, 2716–2718; c) A. Caneschi, A. Cornia, S. J. Lippard, G. C. Papaefthymiou, R. Sessoli, *Inorg. Chim. Acta* **1996**, *243*, 295–304.

[10] a) A. Cornia, D. Gatteschi, K. Hegetschweiler, L. HausherrPrimo, V. Gramlich, *Inorg. Chem.* **1996**, *35*, 4414–4419; b) J. Spandl, M. Kusserow, I. Brudgam, *Z. Anorg. Allg. Chem.* **2003**, *629*, 968–974.

[11] a) P. C. Healy, J. M. Patrick, A. H. White, *Aust. J. Chem.* **1984**, *37*, 1405–1410; b) S. Parsons, G. A. Solan, R. E. P. Winpenny, *J. Chem. Soc., Chem. Commun.* **1995**, 1987–1988; c) J. M. Vincent, S. Menage, J. M. Latour, A. Bousseksou, J. P. Tuchagues, A. Decian, M. Fontecave, *Angew. Chem. Int. Ed. Engl.* **1995**, *34*, 205–207; d) C. Duboc-Toia, S. Menage, J. M. Vincent, M. T. Averbuch-Pouchot, M. Fontecave, *Inorg. Chem.* **1997**, *36*, 6148–6149.

[12] F. Neese, *J. Phys. Chem. Solids* **2004**, *65*, 781–785.

[13] A. L. Spek, *PLATON, A Multipurpose Crystallographic Tool*, Utrecht University, Utrecht, The Netherlands, **2000**.

[14] G. M. Sheldrick, *SHELXS-97*, *Program for Crystal Structure Resolution*, University of Göttingen, Göttingen, Germany, **1997**.

[15] G. M. Sheldrick, *SHELXL-97*, *Program for Crystal Structure Analysis*, University of Göttingen, Göttingen, Germany, **1997**.

[16] M. J. Frisch, G. W. T., H. B. Schlegel, G. E. Scuseria, M. A. Robb, J. R. Cheeseman, J. A. Montgomery Jr, T. Vreven, K. N. Kudin, J. C. Burant, J. M. Millam, S. S. Iyengar, J. Tomasi, V. Barone, B. Mennucci, M. Cossi, G. Scalmani, N. Rega, G. A. Petersson, H. Nakatsuji, M. Hada, M. Ehara, K. Toyota, R. Fukuda, J. Hasegawa, M. Ishida, T. Nakajima, Y. Honda, O. Kitao, H. Nakai, M. Klene, X. Li, J. E. Knox, H. P. Hratchian, J. B. Cross, C. Adamo, J. Jaramillo, R. Gomperts, R. E. Stratmann, O. Yazyev, A. J. Austin, R. Cammi, C. Pomelli, J. W. Ochterski, P. Y. Ayala, K. Morokuma, G. A. Voth, P. Salvador, J. J. Dannenberg, V. G. Zakrzewski, S. Dapprich, A. D. Daniels, M. C. Strain, O. Farkas, D. K. Malick, A. D. Rabuck, K. Raghavachari, J. B. Foresman, J. V. Ortiz, Q. Cui, A. G. Baboul, S. Clifford, J. Cioslowski, B. B. Stefanov, G. Liu, A. Liashenko, P. Piskorz, I. Komaromi, R. L. Martin, D. J. Fox, T. Keith, M. A. Al-Laham, C. Y. Peng, A. Nanayakkara, M. Challacombe, P. M. W. Gill, B. Johnson, W. Chen, M. W. Wong, C. Gonzalez, J. A. Pople, *Gaussian 03*, Revision D.01, Gaussian, Inc., Pittsburgh PA, **2003**.

[17] a) L. Noodleman, *J. Chem. Phys.* **1981**, *74*, 5737–5743; b) L. Noodleman, E. J. Baerends, *J. Am. Chem. Soc.* **1984**, *106*, 2316–2327.

[18] T. Soda, Y. Kitagawa, T. Onishi, Y. Takano, Y. Shigeta, H. Nagao, Y. Yoshioka, K. Yamaguchi, *Chem. Phys. Lett.* **2000**, *319*, 223–230.

[19] a) E. Ruiz, J. Cano, S. Alvarez, P. Alemany, *J. Comput. Chem.* **1999**, *20*, 1391–1400; b) E. Ruiz, A. Rodriguez-Fortea, J. Cano, S. Alvarez, P. Alemany, *J. Comput. Chem.* **2003**, *24*, 982–989.

[20] E. A. Schmitt, L. Noodleman, E. J. Baerends, D. N. Hendrickson, *J. Am. Chem. Soc.* **1992**, *114*, 6109–6119.

[21] H. F. King, R. E. Stanton, H. Kim, R. E. Wyatt, R. G. Parr, *J. Chem. Phys.* **1967**, *47*, 1936–1941.

[22] S. Sinnecker, F. Neese, L. Noodleman, W. Lubitz, *J. Am. Chem. Soc.* **2004**, *126*, 2613–2622 and references therein.

Received: March 31, 2008
Published Online: July 25, 2008

